Water Research Resources

Supporting Information for

Effects of climate change on inter-basin exchange in Lower Lake Constance

I. Caramatti[1], H. Hofmann[1] and F. Peeteers[1]

1 University of Konstanz, Konstanz, Germany

Contents of this file

Text S1 to S9
Figures S1 to S22
Tables S1 to Sx6

Introduction

The Supporting Information includes text, figures and tables that illustrates:

- the set-up of the coarse model of LC (Text S1) and the derived water temperature of the river Seerhein (Fig. S1)
- the model validation in LLC (Text S2-S3, Fig. S2 – S3, Tab. S1)
- the simulated lake thermal structure in GS and ZS (Fig. S4 – S7, Tab. S2 – S3)
- the grid of the COSMO windfield and the seasonal pattern of wind at the sill (Text S4, Fig. S8 – S9)
- the statistical analysis used to investigate potential links between parameters (Text S5 – S7, Tab. S4 – S6)
- the comparison of currents at the sill and at the station M_{GS} and M_{ZS} (Text S8, Fig. S10 – S12)
- the results of the sensitivity analysis (Text S9, Fig. S13)
- the maximum ice coverage of the lake surface in the scenarios (T0, W+ and W-) (Fig. S14)
- the seasonal water level scenarios and the results in the reference scenario W_m (Fig. S15-S16)
- the results of the tracer experiments (Fig. S17 – S22)

Text S1.

The hydrodynamic model of LC used to derive the inflow temperature of the Seerhein was previously set up and validated in Caramatti et al. (2019). The model was characterized by a 300 m x 300 m horizontal grid and 70 vertical layers of variable thickness. The vertical resolution was 1 m in the upper 29 layers and 10 m in the lower 10 layers. Between the 30th and 57th layer the vertical resolution varied slowly between 1 and 10 m. The major inflows of LC, according to Stewart (1988), were considered and the water level was kept constant to the mean water level during the simulated period (396 m.a. s. l.), by adjusting the outflow discharge with a water balance.

Water temperature in LC was initialized by means of data from a thermistor chain (RBR-solo, vertical resolution 0.5 to 2 m in the upper 20 m and coarser below) at the station EU, the deepest station in the Überlingen basin of ULC, and data with a coarser resolution (from 5 to 20 m) from the Landesanstalt fuer Umwelt Baden-Wuerttemberg (LUBW) at station FU (the deepest point of ULC), M_{GS}, M_{ZS} and M_{RH}. Horizontally resolved wind fields (COSMO-MeteoSwiss, resolution 2.2 km until August 2016 and then 1.1 km) were linearly interpolated to the computational grid of LC. Except for the wind field, the model was driven with horizontally uniform meteorological data. For the climate warming scenario (T4) the model was run with increased air temperature (+4°C) and increased inflow temperature (95% of the increase in air temperature). The new initial conditions were derived after a pre-run repeating the meteorological and flow conditions of the year 2009 in a warmer scenario.

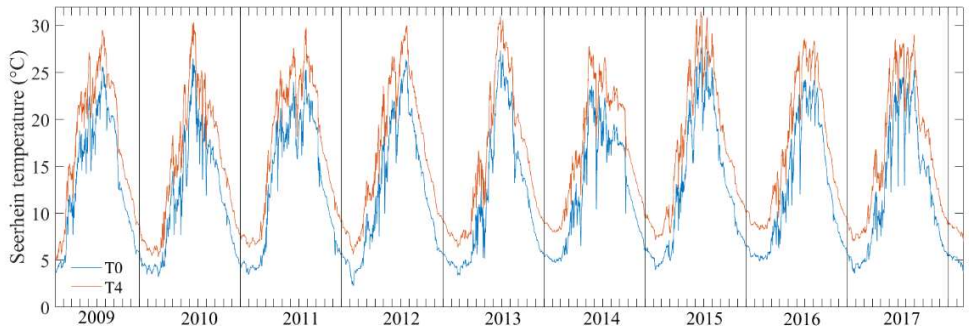

Figure S1. Simulated multi-annual course of Seerhein temperature in the scenarios T0 and T4.

Text S2.

Model results and observations of water temperature were compared at the two stations M_{GS} and M_{ZS} for three consecutive years (2010, 2011, and 2012) to validate the model performance in terms of thermal structure throughout the season and among years (Fig. S2).

The agreement between simulated thermal structure and monthly temperature profiles was evaluated using the root mean square error (RMSE). A mean RMSE was computed for each of the four periods described above (December-March, April-May, June-September, October-November) and is presented in Tab. S1. The model represents the thermal structure most accurately between October and March, with a mean RMSE between 0.37 and 1.08°C in ZS and 0.97 and 1.82°C in GS. During the winter months (from December-March), the mean RMSE was 0.85, 0.37, 0.45°C in ZS for the years 2010, 2011, 2012 and 1.03, 0.98°C in GS for the years 2010, 2012 (no data available in 2011). The simulation was least accurate in the period June-September, with a maximum mean RMSE of 1.49 at MZS and 2.34°C at M_{GS}. In each case, the model reproduced the thermal structure more accurately at station M_{ZS} than at M_{GS}. Text published in caramatti et al. (2020).

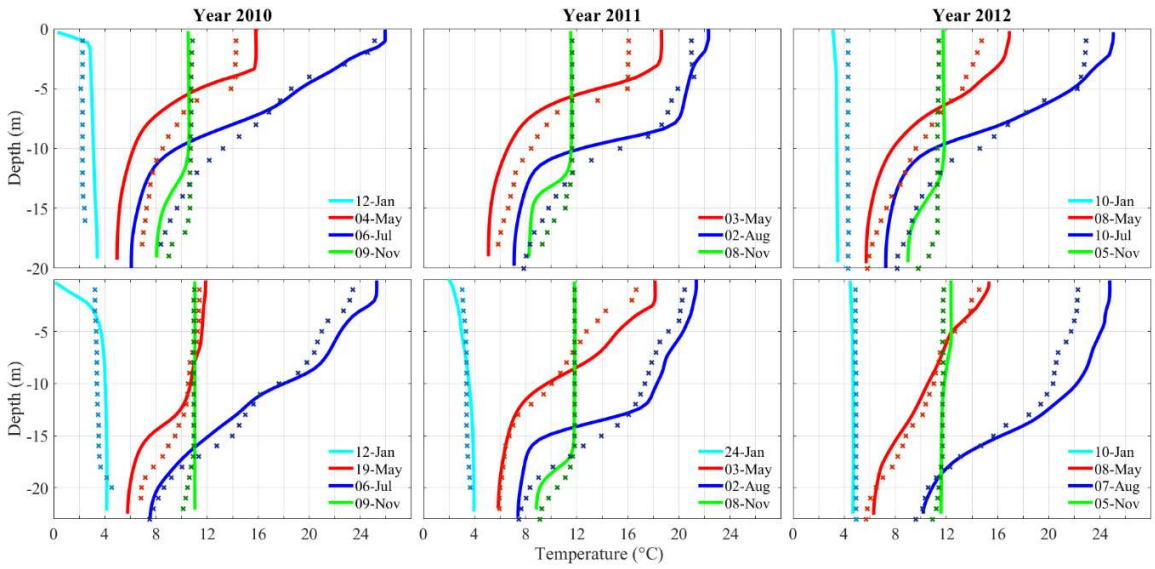

Figure S2. Model validation: Seasonal differences in thermal structure between observed (continuous line) and simulated (dotted line) temperature in Gnadensee (GS) and Zeller See (ZS) for characteristic snapshots of three consecutive years (2010, 2011 and 2012). Figure published in Caramatti et al. (2020).

Gnadensee				
RMSE (°C)	Dec. - March	April - May	June – Sept.	Oct. – Nov.
2010	1.03	2.16	2.26	1.03
2011	-	2.01	2.06	1.82
2012	0.98	1.59	2.34	0.97

Zeller See				
RMSE (°C)	Dec. - March	April - May	June – Sept.	Oct. – Nov.
2010	0.85	1.12	1.32	1.02
2011	0.37	0.97	2.22	1.08
2012	0.45	0.51	1.49	0.35

Table S1. Model validation based on temperature. RMSE between measured and simulated temperature profiles of the sub-basins Gnadensee and Zeller See. Table published in Caramatti et al. (2020).

Text S3.

The simulated current velocities across the sill between Gnadensee (GS) and Zeller See (ZS) were compared with field measurements taken with an Aquadopp HR Profiler (Nortek) at position M_{AQ} (Fig. S3). The field instrument was looking upward measuring between 0.7 – 1.7 m above the ground (mean water depth: 2.5 m) with a high vertical resolution of 0.05 m and a sampling rate of 5 s. Field data was collected between 7/7/2018 – 28/11/2018. The model output was extrapolated at the position M_{AQ} and at the depth investigated by the Aquadopp. The simulated components of the current velocity were interpolated to the time of the field measurements (1 hour interval). Both time series were then smoothed weekly and thereafter the RMSE between model and data was calculated.

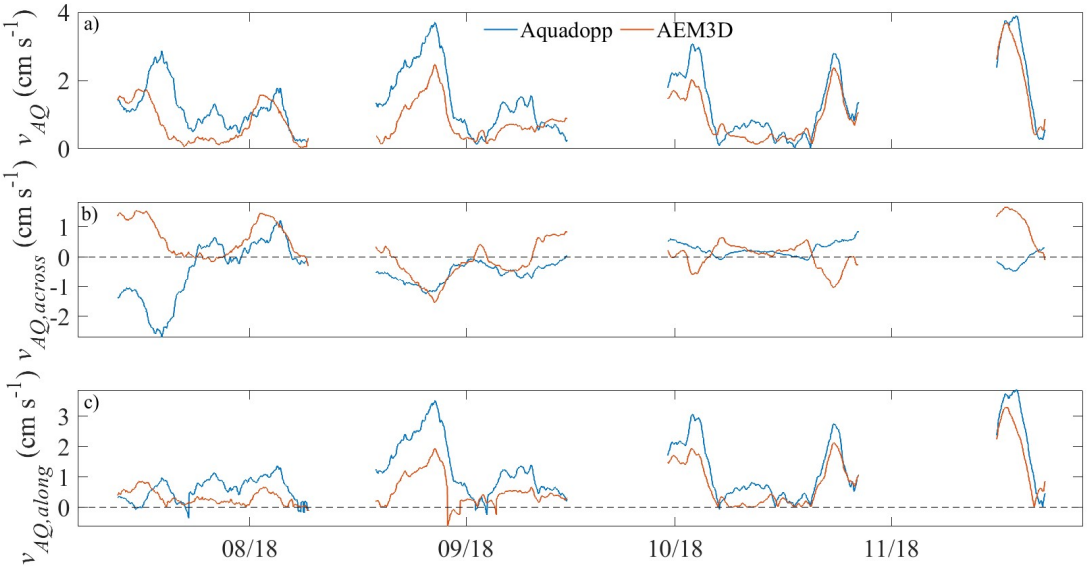

Figure S3. Model validation of currents across the sill between GS and ZS. Comparison between observed (blue) and simulated (orange) current speed (v_{AQ}), as well as the along- and across-velocity components ($v_{AQ,along}$ and $v_{AQ,across}$) at station M_{AQ} with respect to $Trans_{M\text{-}R}$.

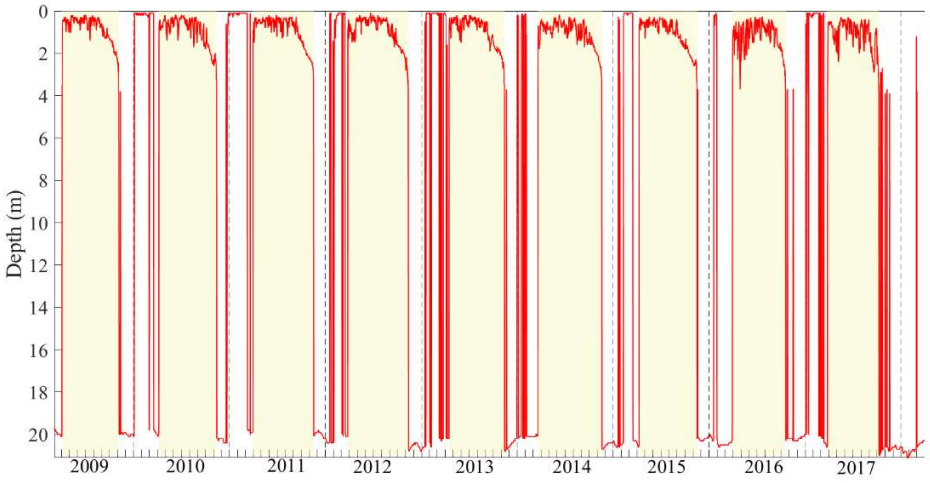

Figure S4. Simulated MLD_{GS}. The duration of the stratification period at M_{GS} is shaded in yellow.

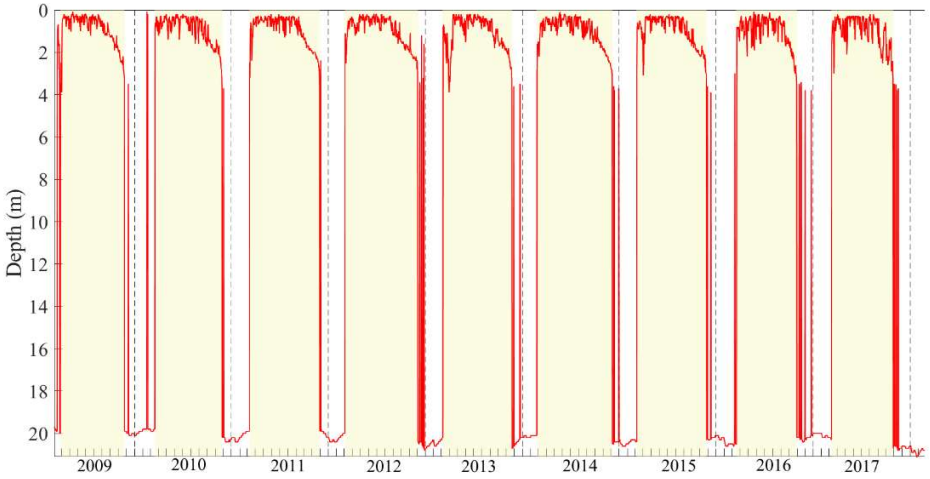

Figure S5. Simulated MLD_{GS} in the scenario T4. The duration of the stratification period at M_{GS} is shaded in yellow.

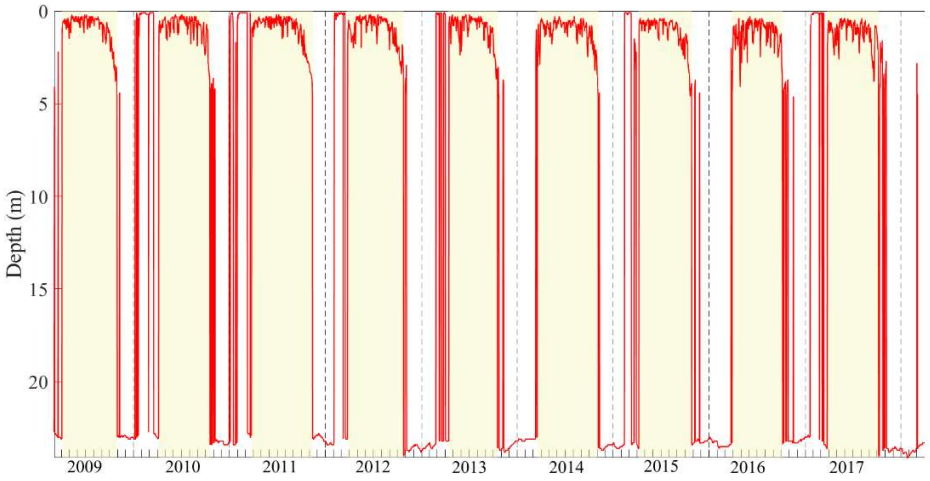

Figure S6. Simulated MLD_{ZS}. The duration of the stratification period at M_{ZS} is shaded in yellow.

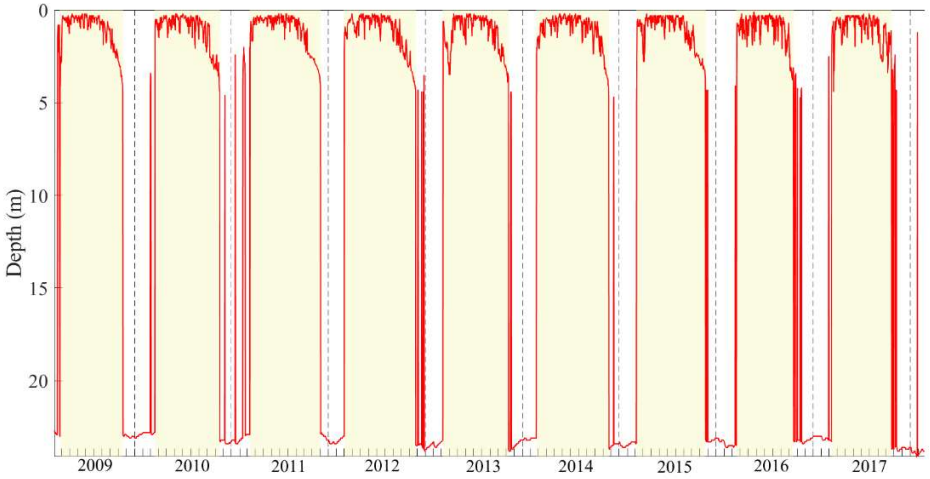

Figure S7. Simulated MLD_{ZS} in the scenario T4. The duration of the stratification period at M_{ZS} is shaded in yellow.

Year	Beginning of stratification (doy)	Ending of stratification (doy)	Duration stratification (days)	Δ Beginning of stratification (days)	Δ Ending of stratification (days)	Δ Duration of stratification (days)
Scenario T0						
2009	91	308	217	-	-	-
2010	95	315	220	-	-	-
2011	88	319	231	-	-	-
2012	84	315	231	-	-	-
2013	104	315	211	-	-	-
2014	77	321	244	-	-	-
2015	98	318	220	-	-	-
2016	88	291	203	-	-	-
2017	84	280	196	-	-	-
Average	90	309	219	-	-	-
Scenario T4						
2009	85	326	241	- 6	18	24
2010	76	329	253	- 19	14	33
2011	69	333	264	- 19	14	33
2012	61	336	275	- 23	21	44
2013	90	325	235	- 14	10	24
2014	53	339	286	- 24	18	42
2015	65	329	264	- 33	11	44
2016	76	304	228	- 12	13	25
2017	68	300	232	- 16	20	36
Average	71	325	253	- 18	15	34

Table S2. Timing and deviation of the summer stratification period between the reference scenario T0 and the climate change scenario T4 at station M_{GS}.

Year	Beginning of stratification (doy)	Ending of stratification (doy)	Duration stratification (days)	Δ Beginning of stratification (days)	Δ Ending of stratification (days)	Δ Duration of stratification (days)
Scenario T0						
2009	91	301	210	-	-	-
2010	94	289	195	-	-	-
2011	83	315	232	-	-	-
2012	83	296	213	-	-	-
2013	103	288	185	-	-	-
2014	75	307	232	-	-	-
2015	97	298	201	-	-	-
2016	87	279	192	-	-	-
2017	83	278	195	-	-	-
Average	88	295	206	-	-	-
Scenario T4						
2009	83	320	237	- 8	19	27
2010	76	320	244	- 18	31	49
2011	69	335	266	- 14	20	34
2012	59	328	269	- 24	32	56
2013	65	312	247	- 38	24	62
2014	52	325	273	- 23	18	41
2015	64	324	260	- 33	26	59
2016	76	291	215	- 11	12	23
2017	68	294	226	- 15	16	31
Average	68	317	249	- 20	22	42

Table S3. Timing and deviation of the summer stratification period between the reference scenario T0 and the climate change scenario T4 at station M_{ZS}.

Text S4.

The COSMO wind field (MeteoSwiss) was linearly interpolated to the computational grid of LLC and ULC. The wind field had a spatial resolution of 2.2 km before August 2016 and afterwards 1.1 km. The north- and east-wind components were derived in the closest points to $Trans_{M\text{-}R}$ of both grids (Fig. S8) to investigate their correlation with the inter-basin water exchange.

Wind components were computed along and across $Trans_{M\text{-}R}$ ($Across_w$, $Along_w$) and then averaged monthly to observe the existence of a wind seasonal pattern. The wind speed, *WS*, and direction, WD, were computed from the monthly-averaged north- and east-wind components.

The wind flows on average south-westwards (from GS to ZS). However, the average speed of the wind flow across and along the sill did not show a pronounced seasonal pattern (Fig. S9).

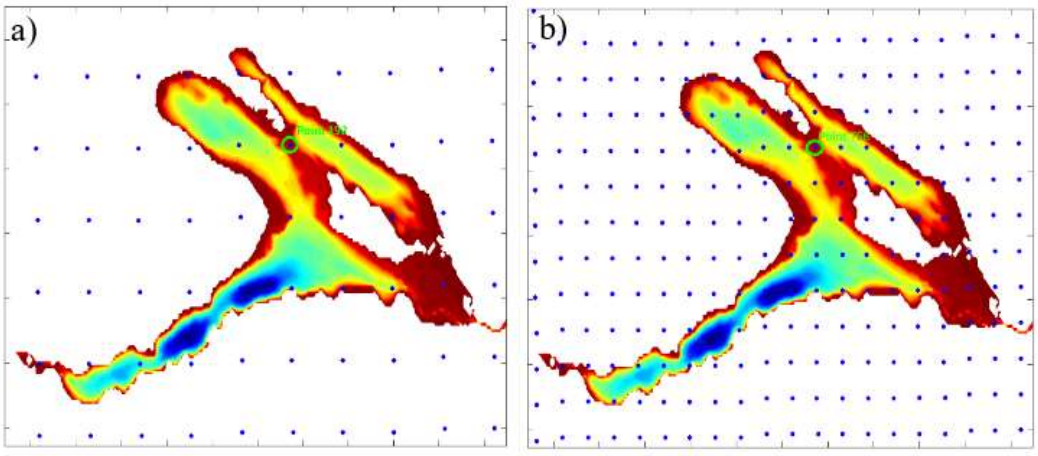

Figure S8. Selected points closest to $Trans_{M\text{-}R}$ of the wind field a) with a 2.2 km (station 192) and b) 1.1 km) resolution (station 766).

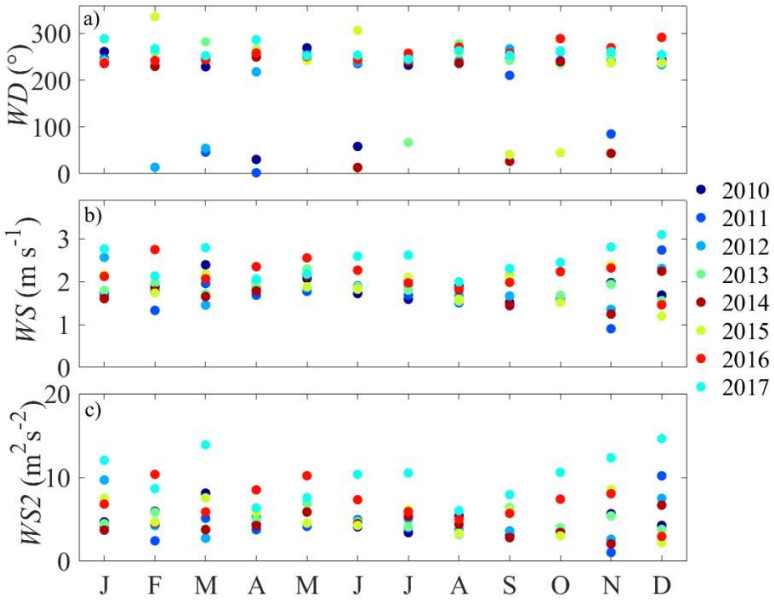

Figure S9. Seasonal pattern of monthly-averaged wind at the grid point of the COSMO windfield closest to $Trans_{M\text{-}R}$ (station 192 and 766). Note that the wind direction *WD* is expressed relative to the north direction and WS2 represents the wind speed squared, which is proportional to the wind forcing at the lake surface.

Text S5.

Linear regression analysis was applied to investigate potential links between V_{exc}, WL_S, A_S, v_s, $MLD_{SI,}$ *WS* (Fig. 4). The analysis was performed using multi-annual averages (January 2010 to December 2017) of monthly-mean data from considering two different data sets: a) considering the ice free season April to December and (b) considering all month.

		r	R^2	p-value
$WL_{S,m}$	$V_{exc,m}$	0.93	0.86	<0.001
$A_{S,m}$	$V_{exc,m}$	0.93	0.86	<0.001
$v_{S,m}$	$V_{exc,m}$	0.99	0.98	<0.001
$MLD_{SI,m}$	$V_{exc,m}$	-0.83	0.69	0.01
$WL_{S,m}$	$v_{S,m}$	0.87	0.77	<0.001
$MLD_{SI,m}$	$v_{S,m}$	-0.82	0.68	0.01
$WL_{S,m}$	$A_{S,m}$	-0.77	0.60	0.01
$MLD_{SI.m}$	$WL_{S,m}$	-0.77	0.60	0.01
$MLD_{SI,m}$	$A_{S,m}$	1.00	1.00	<0.001
WS_m	$V_{exc,m}$	0.24	0.06	0.54
WS_m	$v_{S,m}$	0.32	0.10	0.40

Table S4. Results from the regression analyses of the seasonal change in multi-annual averages of monthly mean values considering the ice free season April to December. The variables included in this analysis are the multi-annual averages (years 2010-2017) of monthly-mean properties water exchange $V_{exc,m}$, water level $WL_{S.m}$, area of the cross-section above along $Trans_{M-R}$ the sill $A_{S,m}$, current speed across $Trans_S$, $v_{s,m}$, mixed layer depth at the station M_{SI} $MLD_{SI,m}$, and wind speed close to the sill WS_m.

		r	R^2	p-value
$WL_{S,m}$	$V_{exc,m}$	0.95	0.91	<0.001
$A_{S,m}$	$V_{exc,m}$	0.95	0.91	<0.001
$v_{S,m}$	$V_{exc,m}$	0.99	0.98	<0.001
$MLD_{SI,m}$	$V_{exc,m}$	-0.56	0.31	0.06
$WL_{S,m}$	$v_{S,m}$	0.92	0.84	<0.001
$MLD_{SI,m}$	$v_{S,m}$	-0.50	0.25	0.10
$WL_{S,m}$	$A_{S,m}$	-0.52	0.27	0.08
$MLD_{SI.m}$	$WL_{S,m}$	-0.52	0.27	0.08
$MLD_{SI,m}$	$A_{S,m}$	1.00	1.00	<0.001
WS_m	$V_{exc,m}$	0.00	0.00	0.99
WS_m	$v_{S,m}$	0.04	0.00	0.89

Table S5. Results from the regression analyses of the seasonal change in multi-annual averages of monthly mean values considering all months. The variables included in this analysis are the multi-annual averages (years 2010-2017) of monthly-mean properties water exchange $V_{exc,m}$, water level $WL_{S.m}$, area of the cross-section above along $Trans_{M\text{-}R}$ the sill $A_{S,m}$, current speed across $Trans_S$, $v_{s,m}$, mixed layer depth at the station M_{SI} $MLD_{SI,m}$, and wind speed close to the sill WS_m.

Text S6.

Linear regression analysis was applied to investigate potential links between V_{exc} and v_s above and below the MLD_S and other properties relevant for water exchange at the sill (WL_S, A_S, MLD_S, WS). The analysis was performed using multi-annual averages (January 2010 to December 2017) of monthly-mean data considering the ice free season April to December.

		r	R^2	p-value
$WL_{S,m}$	$V_{exc,ML,m}$	0.17	0.03	0.67
$MLD_{SI,m}$	$V_{exc,ML,m}$	0.28	0.08	0.47
$WL_{S,m}$	$V_{exc,B,m}$	0.92	0.85	<0.001
$MLD_{SI,m}$	$V_{exc,B,m}$	-0.92	0.84	<0.001
$WL_{S,m}$	$v_{S,ML,m}$	0.88	0.77	<0.001
$MLD_{SI,m}$	$v_{S,ML,m}$	-0.87	0.76	<0.001
$WL_{S,m}$	$v_{S,B,m}$	0.90	0.81	<0.001
$MLD_{SI,m}$	$v_{S,B,m}$	-0.92	0.84	<0.001

Table S6. Linear regression analysis of the seasonal change V_{exc} and v_S above and below the mixed layer depth along $Trans_{M\text{-}R}$, MLD_S, as function of water level and mixed layer depth at M_{SI}, MLD_{SI}. Analyses are based on multi-annual average monthly-mean data and consider only the ice-free season from April to December.

Text S7.

Climate warming induced changes in monthly mean current speed across the sill (Δv_S, $\Delta v_{S,ML}$, $\Delta v_{S,B}$) and in water exchange (ΔV_{exc}, $\Delta V_{exc,ML}$, $\Delta V_{exc,B}$) were compared to changes in monthly *MLD* at the station M_{SI} (ΔMLD_{SI}) using linear regression analysis (Tab. S6). The change of a property indicated by Δ is the monthly mean difference between the value of this property in scenario T4 minus its value in scenario T0. The regression analyses only consider the ice-free season from April to December.

		r	R^2	p-value
ΔMLD_{SI}	$\Delta Vexc$	-0.46	0.21	0.21
ΔMLD_{SI}	$\Delta V_{exc,ML}$	0.59	0.35	0.09
ΔMLD_{SI}	$\Delta Vexc_{,B}$	-0.82	0.67	0.01
ΔMLD_{SI}	Δv_S	-0.51	0.26	0.16
ΔMLD_{SI}	$\Delta v_{S,ML}$	-0.60	0.36	0.09
ΔMLD_{SI}	$\Delta v_{S,B}$	-0.87	0.76	<.0.001

Table S6. Results on from a linear regression analysis comparing the impact of climate warming on water exchange and on exchange velocity with the corresponding change in mixed layer depth at the deepest station on the sill ($\Delta\ MLD_{SI}$) Analyses are based on monthly-mean data. Δ indicates the difference between the monthly mean value in scenario T4 minus its value in scenario T0. The linear regression considered only the ice-free season from April to December

Text S8.

The vertical and seasonal pattern of the simulated currents at the sill were compared with the simulated currents at the stations M_{GS} and M_{ZS}. The vertical profiles of current speed in M_{GS}, M_{ZS} and M_{SI}, and the across speed component at M_{SI} were averaged monthly and between the years 2010 - 2017. The profiles were then compared in the months July and December, as representative of stratified and fully-mixed water column (Fig. S10a-d).

Additionally, we vertically averaged the monthly-mean current speeds at M_{GS}, M_{ZS} and M_{SI}, and the across speed component at M_{SI} to compare the seasonal pattern in the open water of Gnadensee and Zellersee and at the deepest station on the sill. The currents speeds were averaged from the water surface to the maximum water depth at the deepest station of the sill.

The vertical current velocity components at M_{GS} and M_{ZS} were compared in three different periods of the year 2010, as representative of the different thermal conditions in the lake: in April (establishment of stratification), in July (stable stratification) and in November (fully-mixed water column). For each month, 10 days were shown in the figures S11 and S12.

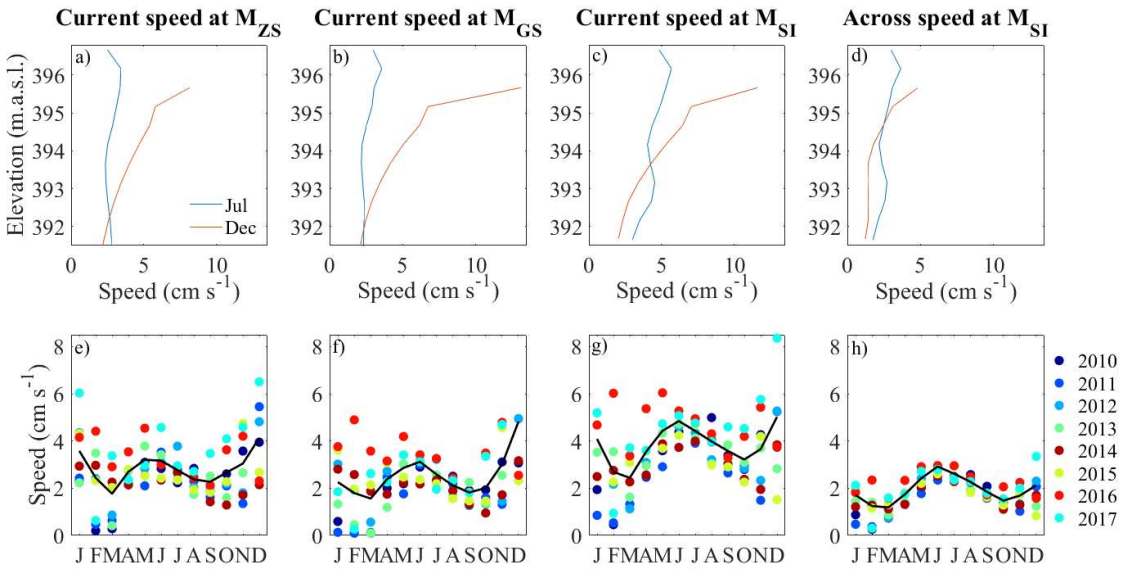

Figure S10. Vertical profiles and seasonal changes of mean currents in the open water of Gnadensee and Zellersee and at the deepest station of the sill. Profiles are multi-annual averages (2010-2017) of monthly mean current profiles for July and December at station a) M_{GS}, b) M_{ZS} and c) M_{SI}. In addition, similarly constructed profiles of the speed of the current across the sill at the deepest station of the sill are depict in d). The symbols in e-h show the monthly mean vertically averaged current speed at e) M_{GS}, f) M_{ZS} and g) M_{SI} and h) of the speed across the sill at M_{SI}. The vertical profiles and the vertical averages extend over the elevation range from the deepest point of the sill to the water surface. The multi-annual averages consider only the depth range available in all years, i.e. from the surface down to the multi-annual minimum of the monthly mean Ds. The black line connects the multi-annual average of the monthly values (years 2010 – 2017).

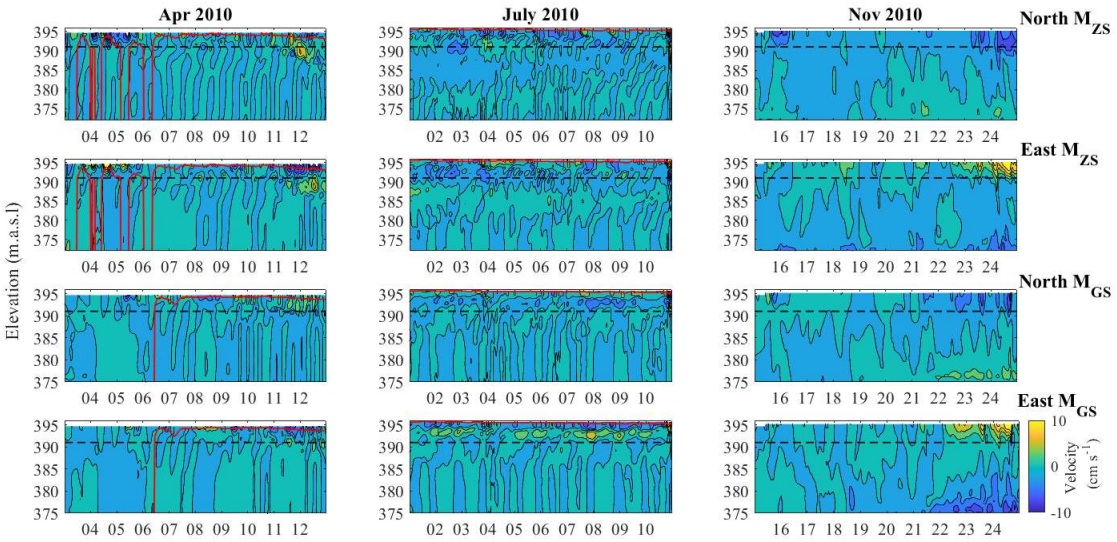

Figure S11. Currents in M_{GS} and M_{ZS}. The north and east components of the current velocity at M_{GS} and M_{ZS} were compared for the year 2010 in April (establishment of stratification), in July (stable stratification) and in November (fully-mixed water column). The mixed layer depth at M_{GS} and M_{ZS} is indicated by a red line, whereas the dashed line refers to the minimum elevation of $Trans_{M\text{-}R}$.

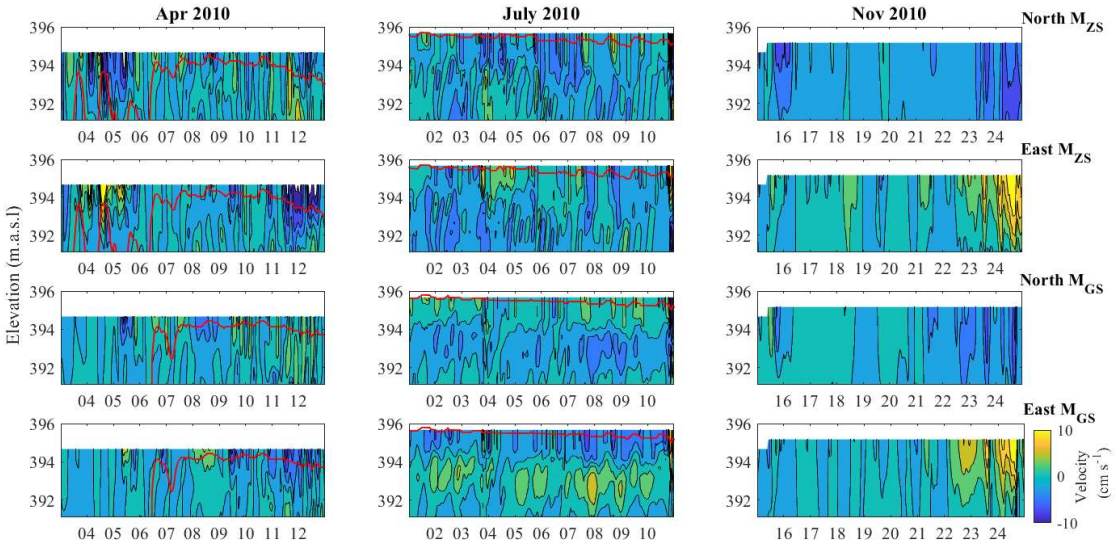

Figure S12. Currents at M_{GS} and M_{ZS} from the surface down to the minimum elevation of $Trans_{M\text{-}R}$. The north and east components of the current velocity at M_{GS} and M_{ZS} were compared for the year 2010 in April (establishment of stratification), in July (stable stratification) and in November (fully-mixed water column). The mixed layer depth at M_{GS} and M_{ZS} is indicated by a red line.

Text S9.

A sensitivity analysis was conducted to investigate the seasonal change of V_{exc} and v_s to relative to the seasonal change in water level by applying a scenario in which the outflow was adjusted to provide a constant water level in LLC with all other conditions being the same as in scenario T0. The year 2010 was used as reference for the analysis. The scenario considered a constant water level from April to December (IO_A).

The response of the system to the scenarios was analyzed at the sill comparing the monthly-mean water exchange (V_{exc}) and mean current speed (v_S) with the reference scenario T0, and at the stations M_{GS} and M_{ZS} comparing the monthly- and vertically-averaged current speed (v_{GZ} and v_{ZS}) of IO_A with T0.

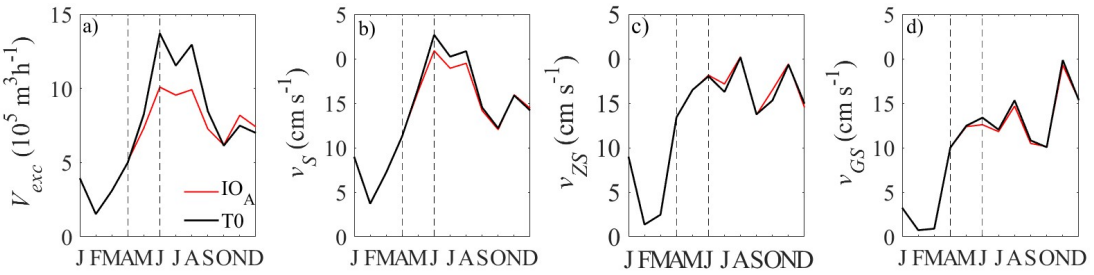

Figure S13. Results of the sensitivity analysis for the year 2010 at the sill and at the stations M_{GS} and M_{ZS}. The reference scenario was T0 (black line). The scenario with constant water level starting in April was called IO_A. The response of the system to the scenarios was analyzed at the sill comparing the monthly-mean water exchange (V_{exc}) and mean current speed (v_S) with the reference scenario, and at the stations M_{GS} and M_{ZS} comparing the monthly- and vertically-averaged current speed (v_{GZ} and v_{ZS}) of IO_A with T0.

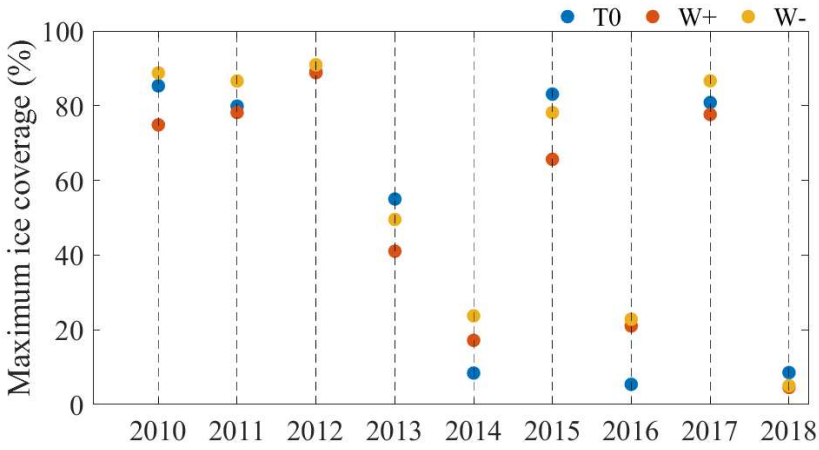

Figure S14. Maximum ice coverage of the lake surface during each winter in the scenarios T0, W+ and W- between 2010 and 2018.

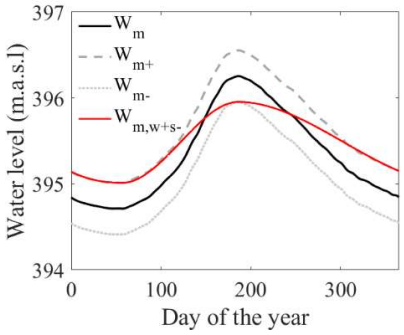

Figure S15. Seasonal water level scenarios. W_m represents the mean seasonal course of water level over the last 200 years which was measured in LLC, whereas $W_{m,w+s-}$ represents a 30 cm higher water level during the winter months and a 0.3 m lower water level during summer. The water level scenario W_{m+} considers a constant increase of 0.3 m with respect to W_m over the year, while W_{m-} a decrease of 0.3 m.

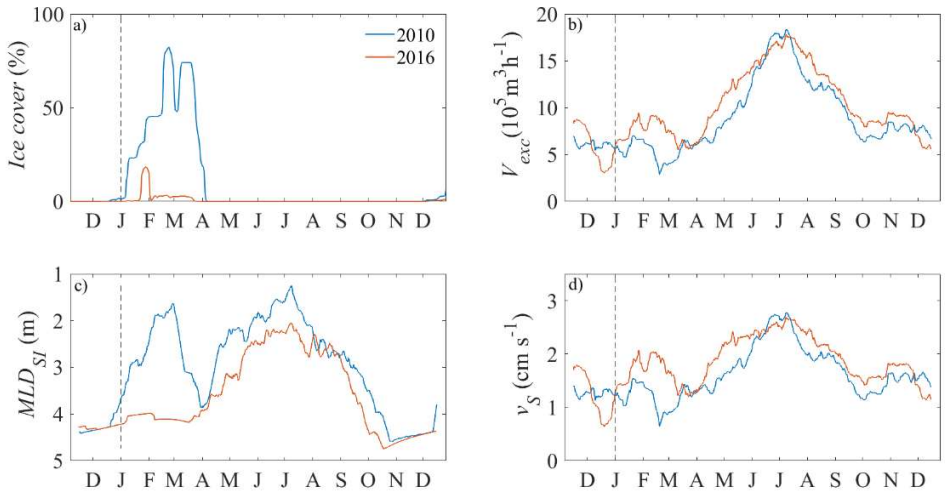

Figure S16. Seasonal course of water exchange V_{exc}, exchange velocity v_s and additional parameters for the scenario W_m. Seasonal pattern of a) percentage of lake surface covered by ice cover, b) water exchange V_{exc}, c) mixed layer depth at M_{SI}, MLD_S, and d) exchange velocity across the sill v_s. Simulation results are provided for the year 2010 (blue), which was characterized by abundant ice cover, and for the year 2016 (red) which was characterized by little ice cover.

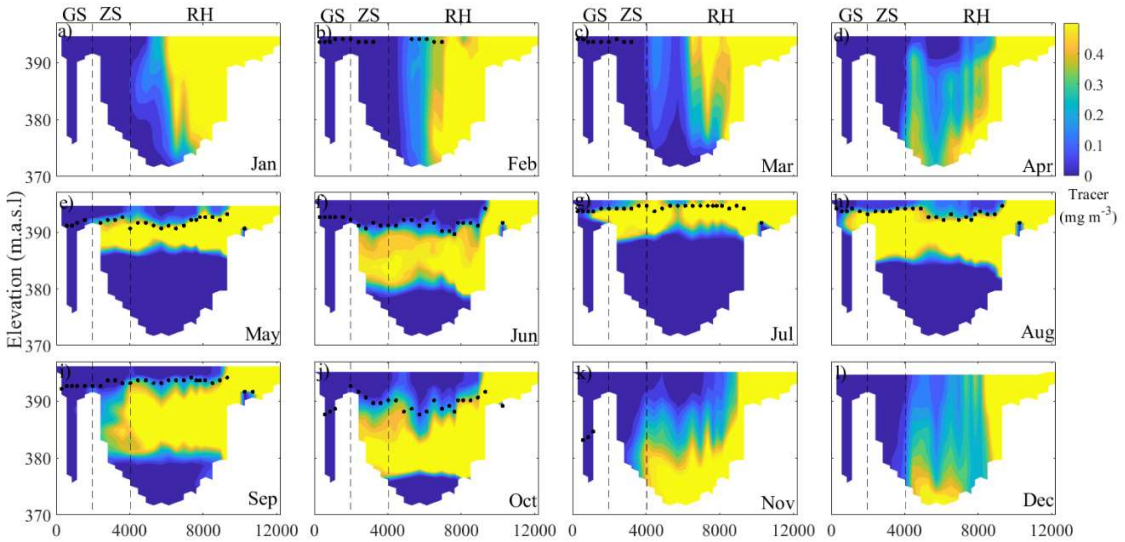

Figure S17. Spreading of the tracer along $Trans_{I\text{-}G}$ for the reference scenario in 2010. Panel a) to l) show the distribution of the tracer concentration 2 days after the beginning of the tracer experiments, which was re-started at the 1st day of each month. The black dots indicate the $MLH_{I\text{-}G}$. The dashed lines delimit the three sub-basins.

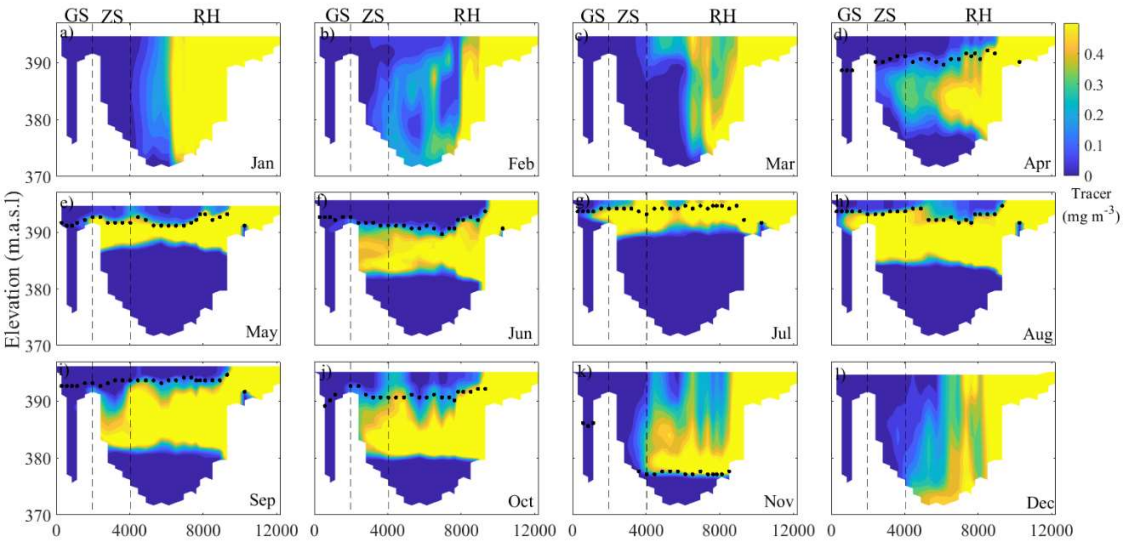

Figure S18. Spreading of the tracer along $Trans_{I\text{-}G}$ for the scenario T4 in 2010. Panel a) to l) show the distribution of the tracer concentration 2 days after the beginning of the tracer experiments,

which was re-started at the 1st day of each month. The black dots indicate the $MLH_{I\text{-}G}$. The dashed lines delimit the three sub-basins.

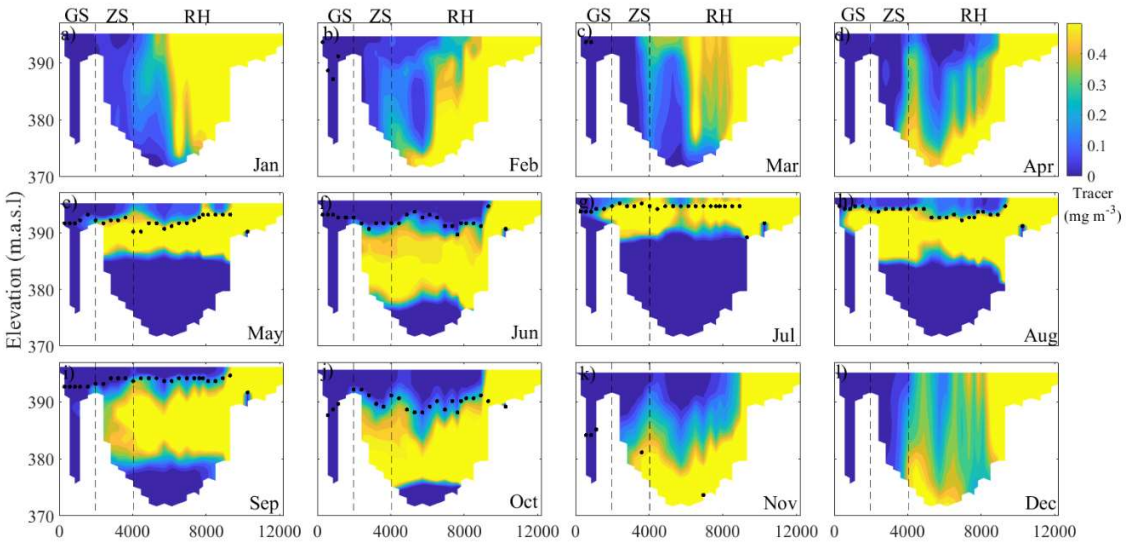

Figure S19. Spreading of the tracer along $Trans_{I\text{-}G}$ for the scenario W+ in 2010. Panel a) to l) show the distribution of the tracer concentration 2 days after the beginning of the tracer experiments, which was re-started at the 1st day of each month. The black dots indicate the $MLH_{I\text{-}G}$. The dashed lines delimit the three sub-basins.

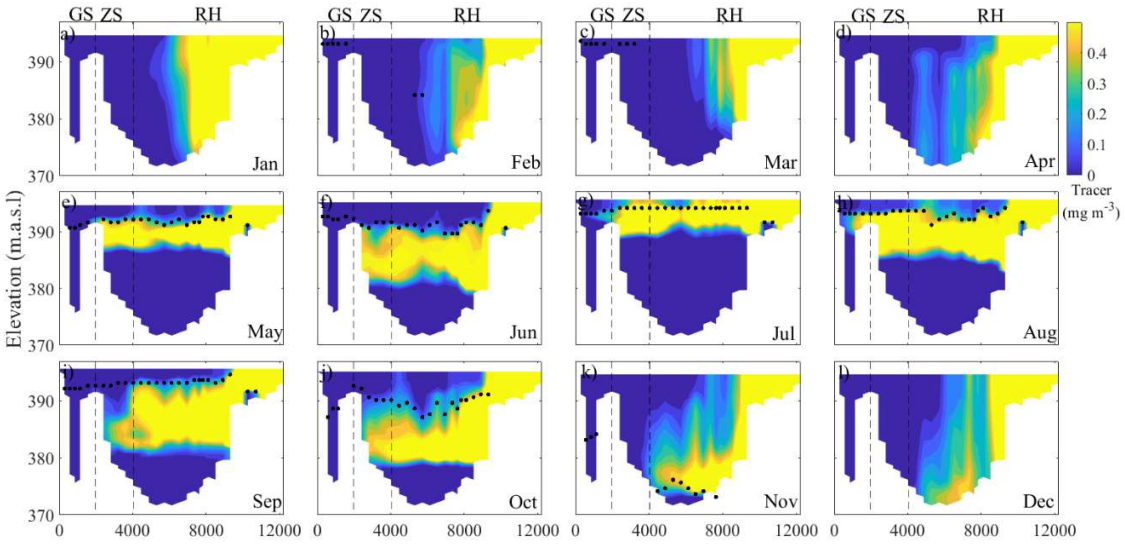

Figure S20. Spreading of the tracer along $Trans_{I\text{-}G}$ for the scenario W- in 2010. Panel a) to l) show the distribution of the tracer concentration 2 days after the beginning of the tracer experiments, which was re-started at the 1st day of each month. The black dots indicate the $MLH_{I\text{-}G}$. The dashed lines delimit the three sub-basins.

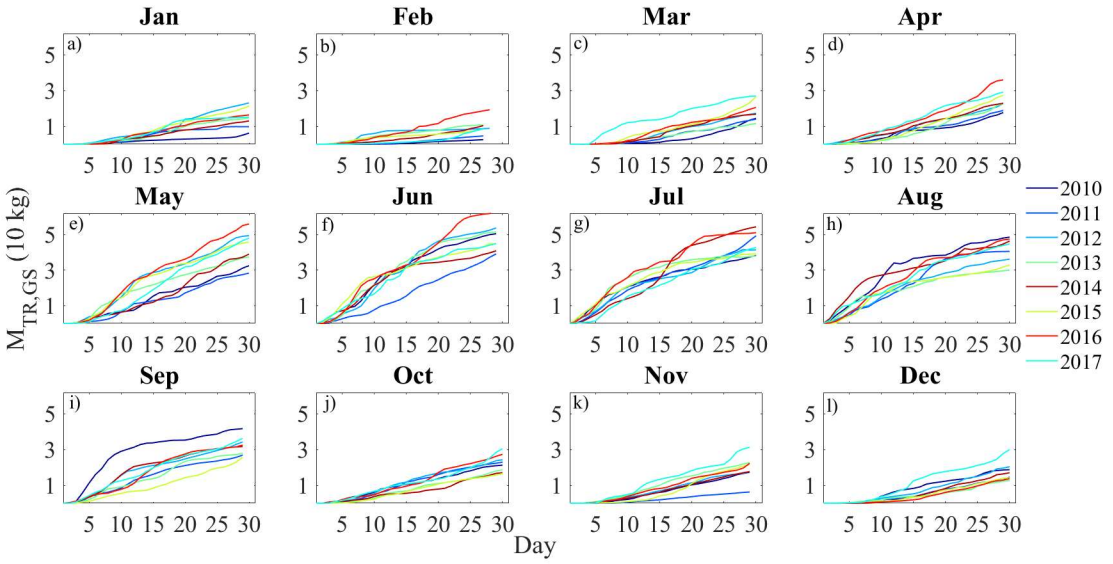

Figure S21. Time series of the tracer mass in GS ($M_{TR,GS}$) for each month and for all years.

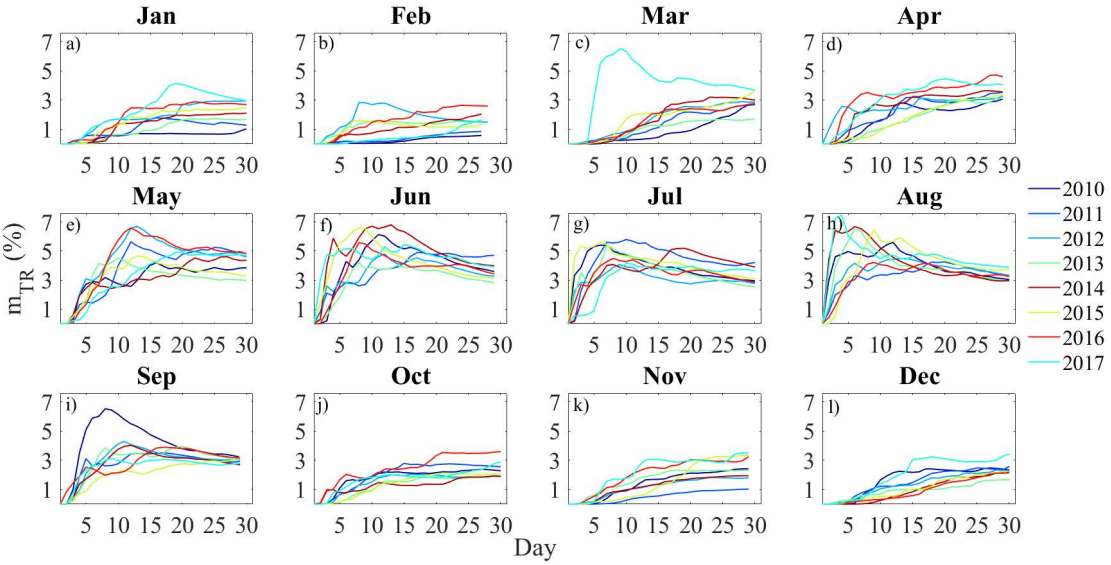

Figure S22. Time series of the fraction of the tracer mass in GS ($M_{TR,GS}$) divided by the mass of tracer introduced in the lake (M_{TR}), i.e. m_{TR} for each month and for all years.